IOP Conf. Series: Materials Science and Engineering **861** (2020) 012016 doi:10.1088/1757-899X/861/1/012016

Simulation of longitudinal surface defect in steel continuous casting

M L S Zappulla and B G Thomas

Mechanical Engineering Department, Colorado School of Mines, 1500 Illinois St, Golden, Colorado, USA, 80401

E-mail: BGThomas@mines.edu

Abstract. Cracks and depressions in steel continuous casting often start during initial solidification in the mold and evolve later in the process. To understand the mechanism(s) of formation of these defects, a finite-element model of transient thermal-mechanical behavior during steel solidification has been developed and applied to simulate longitudinal depressions. The thermal model features a detailed analysis of heat transfer across the interfacial gap, which is fully coupled with a thermal-mechanical elastic-viscoplastic finite-element model that calculates the evolving size and shape of surface depressions. The results are compared with analysis of a sample with a longitudinal surface depression and crack from a commercial continuously cast slab. In this scenario, a thermal event caused a local drop in heat transfer, followed by frictional tension on the domain due to slab shrinkage, led to shell necking and the formation of a localized U-shaped depression. Finally, a new visualization methodology has been developed to better reveal defect formation in real time, such as longitudinal depressions, which persist as they move down the mold at the casting speed.

1. Introduction

Quality during continuous casting is greatly affected by heat transfer across the interfacial gap between the copper mold walls and the steel strand, which governs initial solidification of the steel shell and the formation of surface cracks and other defects [1–3]. Previous work has shown that cracks correlate with high and/or variable heat flux in the mold, especially near the meniscus region [4]. Thus, quality monitoring systems routinely include the measured mold heat flux signal, based on heat up of the cooling water as it passes through the mold as well [5, 6] as well as other methods [6–8].

Combining advanced computational modeling with careful plant measurements and forensic analysis of defects is an important methodology to identify how the defects form. Online visualization of real-time measurements is a useful tool to identify defect formation, hopefully in time to take corrective action, and is better if augmented by calculations based on the defect formation mechanism. This paper presents benchmark measurements obtained during continuous casting when longitudinal depressions and cracks formed, and compares the measurements with corresponding predictions of a thermal-stress model.

2. Benchmark plant measurements

On June 18, 2017, a campaign of low-carbon steel was cast at ~1.4 m/min at slab caster 21 at Tata Steel Europe in Ijmuiden, Netherlands. For this campaign, the loose broad face mold copper was instrumented with a 38 x 70 grid of fiber Bragg grating thermocouples that recorded temperature histories at more

than 2000 locations [9]. The instrumented region extended across the entire mold width from above the meniscus (90mm below top of mold) to 285 mm below the meniscus. Although such molds are complex, and expensive to make and maintain, this new methodology enables faster response time, and smaller spacing between sensors than conventional thermocouples, which can be presented in real time, and recorded with high resolution [10,11]. Figure 1 shows severe longitudinal depressions and cracks in a ~1300 mm-wide slab Z9407-101, which is a relatively rare occurrence. Of particular interest is the depression at ~265 mm from the North narrow face, (-394 mm from the strand centerline), which is about 250 mm long.

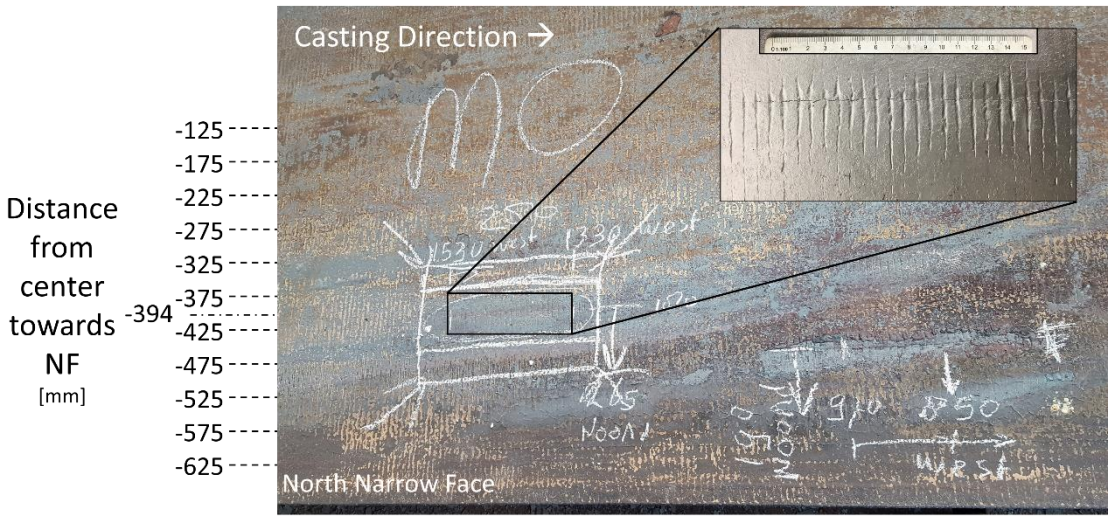

Figure 1. Top surface appearance of slab Z9407-101 with severe longitudinal defects off the North NF and inset image of a slab sample containing a depression that was subjected to detailed metallurgical analysis.

Figure 2 shows the instantaneous temperature profiles measured across the mold subsurface at several times during the casting campaign, which correspond to the ~25 s time period that the 250 mm-long longitudinal depression of interest was in the instrumented portion of the mold. The resolution of the data is indicated by the straight-line segments plotted between measured points, which are sufficiently dense to capture the real profile behavior under most conditions. Figure 2(a) shows typical steady-state temperatures across and down the mold after conditions returned to normal. As expected, temperatures in the mold generally decrease with distance below the meniscus, and steeply decrease towards the narrow faces, (strand corner), indicating the cast width of the strand.

Most importantly, temperatures recorded near to the depression location are lower. Figure 2(b) shows temperatures before, during, and after the residence time of the defect in the mold. It reveals a region of lower temperature that persisted across the mold width during the transient time that the depression developed, which is the general thermal signature of this type of defect. This temperature dip is partly due to the thermal event that initiated the defect and partly due to the consequent drop in heat transfer across the locally larger interfacial gap between the strand and mold wall, which thus experiences a larger thermal resistance. These temperature variations also fluctuate in time.

The center of the depression at -394 mm in figure 1, shown as a dashed vertical line in figure 2(b), passed between two columns of FBG sensors at -375 and -425 mm from the broad face center. A time average of the temperature history over the 30s duration of the depression is shown as a red line in figure 3(b), taken at the FBG sensor column at -375 mm from the wideface centerline, which was closest (~19 mm away) to the depression center (solid vertical line in figure 2(b)). Instantaneous time-averaged far field temperatures were taken at +475mm (opposite side of the slab) and are shown in black in figure 3(a). This temperature profile quantifies the significant drop in temperature from above the meniscus to the end of instrumentation, where it approaches back to the far field value.

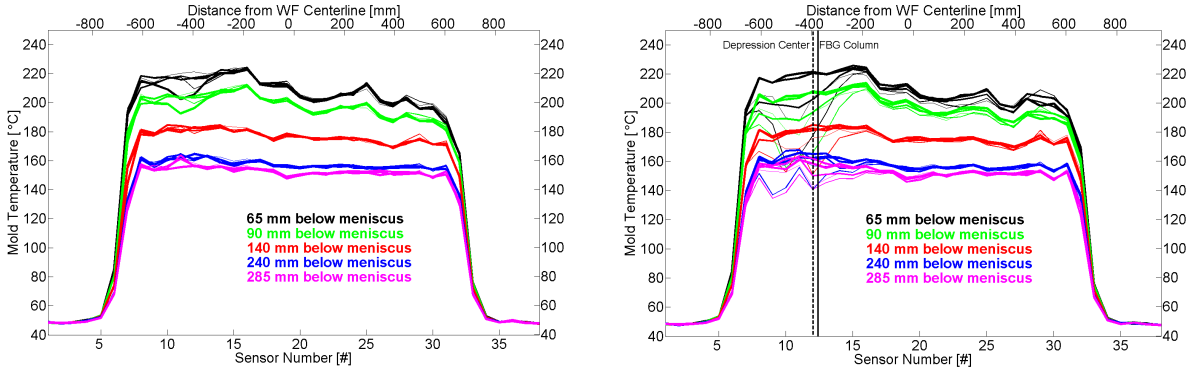

(a) (b)

Figure 2. Measured local temperature profiles across the mold width at specific times and locations down the mold. (a) Uniform casting conditions after the region containing the defect and (b) Before, during, and immediately after formation of the defect region with the depression.

3. Mold data mapping methodology

A new methodology has been developed to better enable operators to interpret continuous online measurement of dense mold temperature data to detect formation of longitudinal defects [12]. Figure 3(b) shows a 3D surface plot of temperatures down the mold for 70 s surrounding the residence time of the surface depression. Lines of constant time run parallel to the axis of distance down the mold. Temperatures are taken from the same vertical line of FBG sensors ~19 mm from the depression center. In this figure, movement in the casting direction at 25 mm/s of two points down the strand in the depression is visualized by two translucent vertical planes, spaced 11s apart. The oldest data is sliced by the right plane, where the shell starts at the meniscus (back right) at 22 s and exits at 37 s.

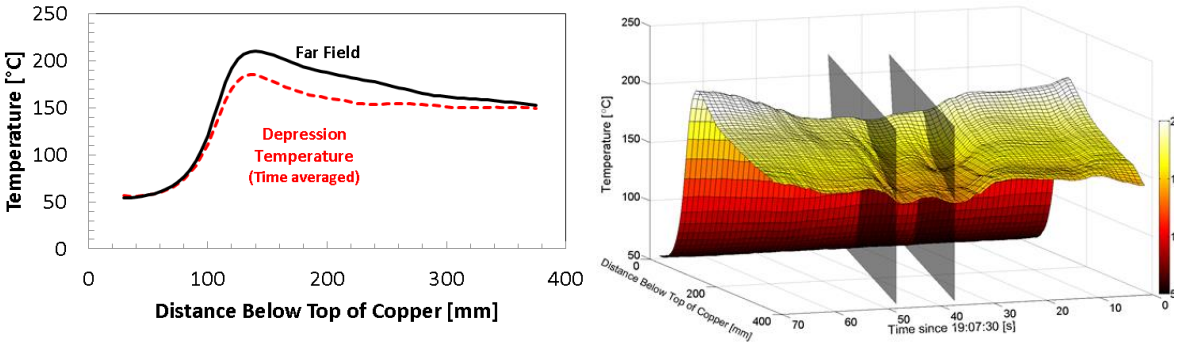

(a) (b)

Figure 3. (a) Temperature profiles down the mold for the far field and the FBG sensor closest to the depression center (19 mm away) averaged over the instrumentation residence time of the depression (b) 3D plot of temperature evolution along the same single vertical line near the depression.

In figure 3(b), there are clearly visible valleys in the temperature plot, delineated by the vertical planes. These temperature valleys represent the time duration of this depression. The angled nature of the valleys matches close to the casting speed planes, which indicates that the depression started at the meniscus and then translated down the strand at the casting speed. The steep gradient near the meniscus on the right plane indicates that the depression formed rapidly; temperatures stayed depressed for ~11 s until the left translucent plane, and then gradually returned to far field conditions. Slight changes in the shape of the valley indicate that the depression shape changed with time, growing rapidly when it first formed, stagnating for a short distance, continuing to grow, and finally receding and disappearing.

3.1. Mapping mold data to slab data

The translating nature of defect formation, shown in the previous section, suggests a better methodology to visualize the formation of defects in the mold. With the high sampling frequency and spatial resolution of FBG molds, it is possible to track detailed time histories that correspond with points on the slab surface moving down the mold at the casting speed, by matching position down the strand according to the time it was adjacent to a given distance down the mold. Then, the instantaneous drop in temperature at a given measured point in the mold surface is found by subtracting T_{Standard}, which is a 2D array of standard temperatures at the instrumented points of the mold, calculated previously by averaging data when no defects occurred, according to the given steel grade and casting conditions:

$$\Delta \mathrm{T(t)} = \min(0, T_{\text{Mold}}(x_{Slab}, y_{Slab} - \int_{t_0}^{t} V_c(t_i)dt_i, t) - T_{\text{Standard}}(x_{Slab}, y_{Slab} - \int_{t_0}^{t} V_c(t_i)dt_i)) \quad (1)$$

While a location of interest on the slab surface, y_{Slab}, is within the instrumented region of the mold, $t_{Enter} < t < t_{Exit}$, the criterion, T_{IDrop}, evolves with time by integrating the history of the temperature drop at that moving location:

$$T_{IDrop}(x_{slab}, y_{slab}, \mathrm{t}) = \int_{t_{Enter}}^{t} \Delta T(t_i)dt_i \quad (2)$$

where t_{Enter} is the time when the location, y_{Slab}, enters the instrumented mold region, $y_{Slab} = y_{Moldtop}$.

Large values of T_{IDrop} at the end of the instrumented region indicate regions of the slab surface which have experienced a mold temperature history that is cooler than standard conditions. This indicates lower heat flux across the interfacial gap and a hotter shell temperature. This is often due to surface depressions, which often lead to cracks, owing to a locally hotter shell. These regions can be tracked, subjected to extra inspection, and perhaps downgraded. This methodology and criterion can be applied to systems with arbitrary spacing of the measurement points, provided there is enough spatial resolution to achieve reasonable accuracy. A contour map of this criterion indicates regions on the strand surface that have experienced prolonged, periods of temperature drops relative to the standard profile, likely due to a surface depression. Details of this methodology are provided elsewhere [12].

3.2. Defect visualization

A console display setup for post-mortem (forensic) defect analysis using this new defect indicator is suggested in figure 4. Figure 4(a) shows the instantaneous contour map in the instrumented region displayed by the sensors at the current time, using a blackbody color map without interpolation.

Figure 4(b) shows a top-down photograph (adjusted to remove perspective) of the final surface appearance of the region of the cast slab corresponding to the temperatures in figure 4(a) at the time it resided in the instrumented region in the mold. The translucent gray rectangle at the top indicates that portion of the image which was above the meniscus level at that time.

Figure 4(c) shows a contour plot of the instantaneous deviations between the standard and current temperatures for each location in the array. Values are always negative or zero, because depression defects always tend to lower mold temperature. Increased negative values indicate deeper depressions.

Figure 4(d) shows an example of the output results from the new methodology, obtained by accumulating the results in figure 4(c) for 11 s (245 mm past the bottom of the instrumented region), according to the new defect criterion function. The time period spent within the instrumented region of the mold is represented by the space between the thick black horizontal lines, labeled top and bottom of instrumentation. Once a surface location passes out of the instrumented region, the contours are fixed, and the calculation for that surface point is completed. Again, increasingly negative numbers indicate higher likelihood of surface quality problems. The longitudinal depression at the left of figure 4(b) is clearly visualized in figure 4(d), but is hardly noticeable in the raw temperature data. This illustrates the value of this new defect identification methodology, which is described in detail elsewhere [12].

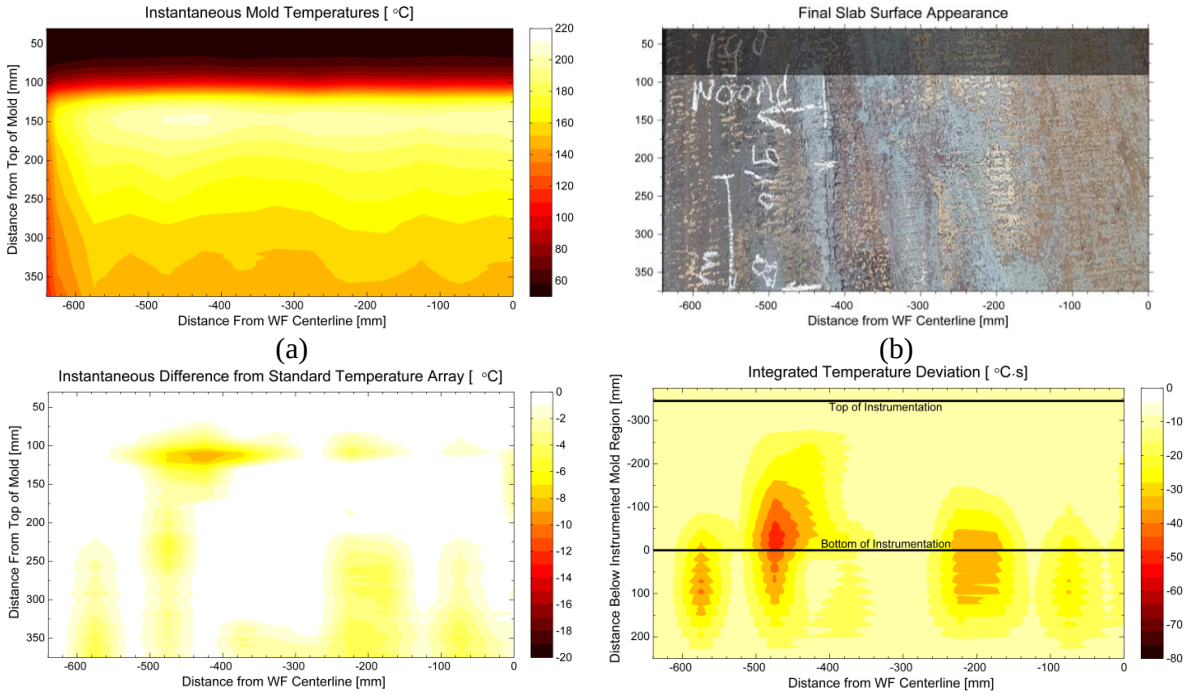

Figure 4. Contours that map defects over half of slab from wide face centerline to narrow face: (a) Instantaneous mold temperature, (b) Final slab surface appearance, (c) Instantaneous difference from standard temperature (d) Defect criterion based on integrated temperature drop, $T_{IdropF.}$.

4. Thermal-mechanical model formulation

The thermal-mechanical model in this work focuses on a two-dimensional (2-D) slice through the solidifying steel shell in a state of generalized plane strain in both x and z directions [3], as it moves down the mold at the casting speed in a Lagrangian reference frame. The model solves the transient heat conduction and momentum equations to predict the temperature, displacement, strain, and stress histories of the shell. The governing equations are solved using the finite-element method in ABAQUS/Standard (implicit). The transient analysis uses coupled-temperature displacement elements and step-wise coupling between the thermal and mechanical calculations. The 20 mm thick x 40 mm wide simulation domain, shown in figure 5(a), represents a portion of the solidifying shell somewhere along the broad face away from the corner.

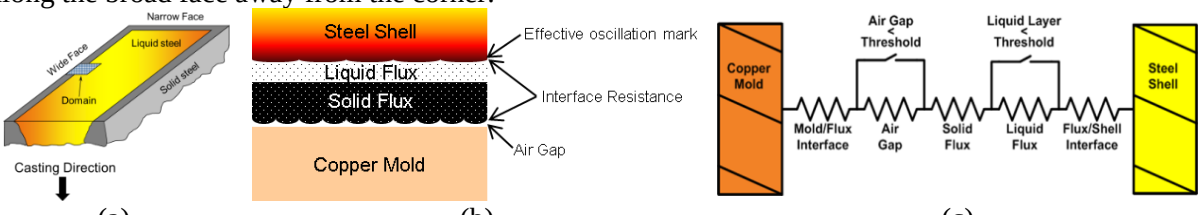

Figure 5. Thermal-stress model domain shown in cutaway of continuously cast slab (a), interfacial gap layers in this model (b), and numerical implementation as a thermal resistor model (c).

The model is applied here to the case with FBG measurements shown in the previous section. The initial temperature is set to the reported tundish temperature, 1554°C in the steel, and 100°C in the mold. Coupling between the solidifying shell and the copper mold was accomplished using a GAPCON subroutine. Given the mold hot face and steel shell surface temperatures, and the total gap thickness calculated by the mechanical model at each time step, the thermal model calculates appropriate local solid and liquid layer thicknesses using: flux solidification temperature 1045°C, and resistances (mm^2

K/mW) of the different layers comprising the gap: the mold/slag interface, 0.0004, air gap, $D_{Air}/0.06$, solid slag layer, $D_{Sol}/3.0$, liquid slag layer, $D_{Liq}/1.0$, and slag/shell interface, $0.251 \exp(-0.0054T_{ls})$. D_{Air}, D_{Sol}, and D_{Liq} are thicknesses of the air gap, solid slag, and liquid slag layers respectively, and T_{ls} is the temperature of the liquid slag/steel shell interface. The slag/shell interface resistance is non-linear and numerically constrained between 1,000 and 20,000 W/K.

To calculate accurate mold temperatures, a Reduced Order Model (ROM) of the mold was applied [13]. Modeled as a single row of elements along the width, the ROM mold has a calibrated thickness of 28.35 mm to account for water slots in the transverse direction. A constant thermal conductivity of 315 W/m·K and variable convection boundary condition is applied to the mold cold face.

The displacement and stress state of the model is calculated by solving the static stress equilibrium equations including frictional contact with μ=0.15. Details of this model, including the elastic-visco-plastic constitutive behavior with different temperature-, and composition-dependent properties in each of the steel phases: liquid, δ-ferrite, and γ-austenite can be found elsewhere [1–3].

5. Thermal model calibration and validation

First, the continuous-casting heat transfer model, CON1D [15] was calibrated to match both the heat flux measured from heat up of the mold cooling water, FBG temperature measurements at the far field, and two rows of embedded thermocouples, as shown in figure 6(a). For these far-field conditions, CON1D suggests a flux layer thickness profile down the gap, as shown in figure 6(b).

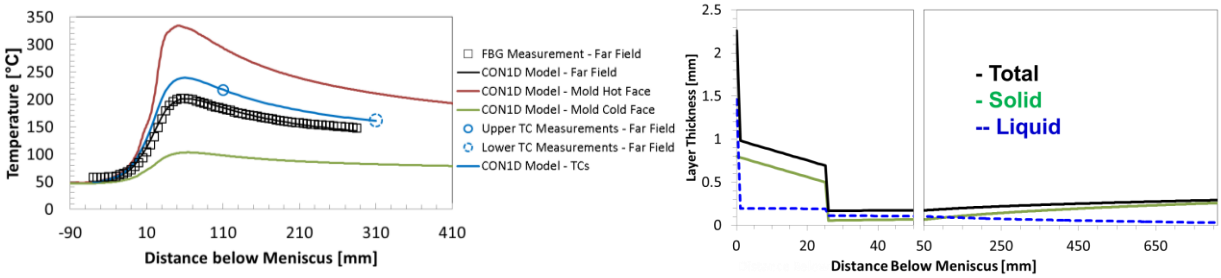

(a) (b)

Figure 6. (a) Temperature results from CON1D with plant measurements for FBG and thermocouples and (b) con1d output results for flux layer composition within the mold.

Of particular interest is that figure 6(b) indicates the presence of a significantly thicker layer of flux extending to 26 mm below the farfield meniscus; Slag thickness then decreases to ~0.2 mm and gradually increases with distance down the mold. The extended slag rim, of ~1 mm thickness, retards heat transfer in the meniscus region, and delays initial formation of the shell below the farfield meniscus. It is needed to enable CON1D to match the plant measurements. This provides strong evidence that such extended slag rims during casting are real. This is further supported by anecdotal evidence from this particular facility where several extended slag rims with similar thickness profiles were found after casting.

After calibration of CON1D with measurements, the GAPCON model in Abaqus was adjusted to match CON1D. Due to the 2D nature of the model, axial heat conduction is neglected. Instead, a negative volumetric heat generation was applied, decreasing from -25 [W/m^3] to zero over the first 10s. Figure 7(a) shows the match with the farfield CON1D heat flux profile, and figure 7(b) shows a comparison with the corresponding mold temperatures, including the FBG data. Note that the peak heat flux appears over 20 mm below the farfield meniscus, owing to the extended meniscus slag rim discussed previously.

Results from the Abaqus model are also compared with the FBG sensor data 19 mm away from the depression center. Figure 7(a) shows that the heat flux profile in the depression center is substantially lower than that of the far field. This is due to the extra thermal resistance created in that region, in

addition to the consequent physical opening of the depression, which was assumed to create an air gap. Figure 7(b) shows a substantially higher peak temperature predicted by the Abaqus model near the meniscus, which is a modeling artifact due to missing copper above the meniscus that removes heat axially and leads to the smoother and lower temperatures of the FBG and CON1D profiles in this plot.

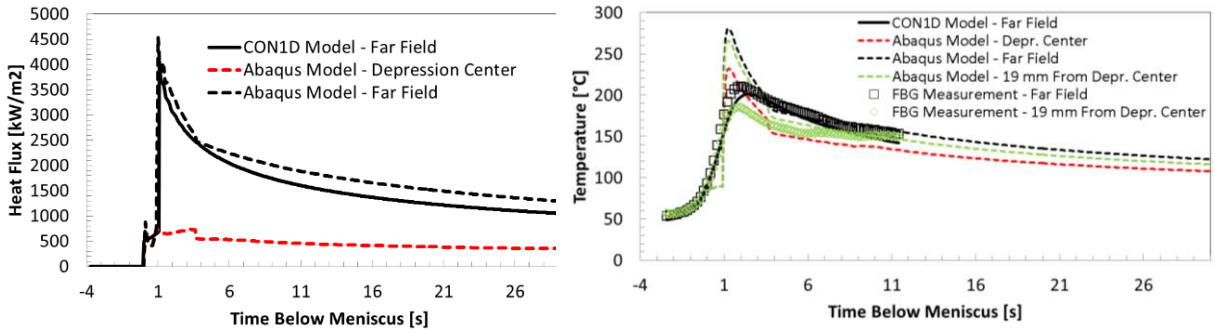

(a) (b)

Figure 7. (a) Calculated heat flux profiles down mold comparing Abaqus and CON1D models; (b) Corresponding mold temperature profiles also comparing with FBG measurements.

6. Thermal-mechanical model results

Depression shape results of the thermal-mechanical model are compared with a digital microscope scan and measurements of the sample in figure 8. The ~4mm deep crack is indicated by the vertical dashed line. The inset compares a micrograph cross section through the depression (right) with the predicted shape (left). The model slightly overpredicts the depression depth, likely due to overprediction of the temperature gradient near the meniscus (figure 7(b)), which is due to incomplete incorporation of the axial heat flow near the meniscus into the Abaqus slice model.

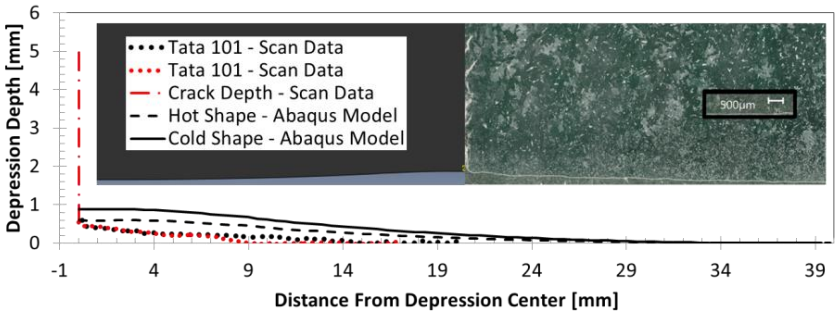

Figure 8. Slab surface depression shape comparing model prediction with scan of sample with defect

Figure 9 shows the results of a parametric study examining the effect of the thermal disruption start location (a); as well as the final deformed shapes, both at mold exit, and after cooling to near ambient (b). The thermal disruption was likely caused by a transient event, such as severe meniscus level fluctuations from turbulent flow. It is observed that delaying the start of the thermal disruption to a lower distance below the meniscus causes the depth of the resultant depression to decrease. It has also been found that the depression stops growing once the surface temperature reaches ~700°C, as shown in figure 9(b), which is substantially deeper than at mold exit. Furthermore, the depression is always much deeper when the disruption starts closer to the meniscus. This finding is consistent with the accepted understanding that longitudinal depressions and cracks tend to initiate close to the meniscus.

7. Conclusions

New models and visualization methods have been developed to enable new insights into the continuous casting solidification process, specifically revealing how temperature differences are related to

longitudinal defect formation. A new computational thermal-stress model has been developed to investigate longitudinal surface defects, as well as to predict the corresponding mold temperatures. Results show that one possible scenario for the specific longitudinal crack and depression defect studied in this case was a ~20 mm wide local thermal disruption, combined with a crack and some applied tension which led to a necking style depression and a U shape defect with a crack at the base.

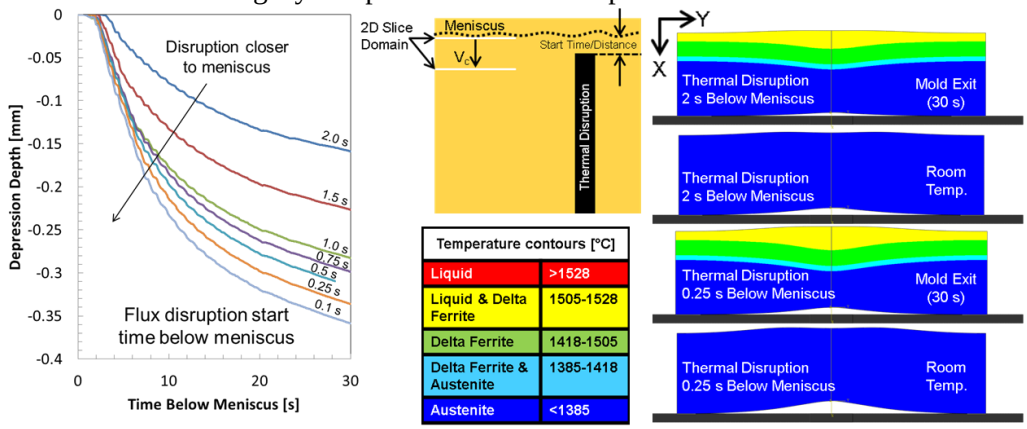

(a) (b)

Figure 9. Effect of thermal disruption initiation time on depression evolution: (a) Depth history for varying disruption initiation times, (b) Deformed shape (scaled 5x) of depression at mold exit and after cooling to near ambient, for late disruption (top) and early disruption (bottom).

Acknowledgements

The authors wish to thank the member companies of the Continuous Casting Center at the Colorado School of Mines for support and plant data. Particular thanks are extended to: Begoña Santillana, Mathias Mul, Ton Spierings, Stephen Carless, Gert Abbel, Dirk Van Der Plas, Arnoud Kamperman, of Tata Steel Europe, and Martin Seden of ABB.

References

[1] Zappulla M L S and Thomas B G 2018 *THERMEC' 2018* (Paris, France)
[2] Zappulla M L S and Thomas B G 2017 *The Materials Society Annual Meeting* **F6** (San Diego, CA) pp 501–10
[3] Zappulla M L S, Hibbeler L C and Thomas B G 2017 *Metall. Mater. Trans. A* **48** 3777–93
[4] Kawamoto M, Tsukaguchi Y, Nishida N, Kanazawa T and Hiraki S 1997 *ISIJ Int.* **37** 134–9
[5] Kumar S, Meech J A, Samarasekera I V, Brimacombe J K and Rakocevic V 1999 *Ironmak. Steelmak.* **26** 269–84
[6] Zhang Y, Vaculik V and Dudzic M 2003 Integrated Monitoring Solution to Start-Up and Run-Time Operations for Continuous Casting *IFAC Proc.* **36** 561–6
[7] Emling W H 2003 *The Making, Shaping and Treating of Steel: Casting Volume* ed A W Cramb (Pittsburgh, PA: AISE Steel Foundation)
[8] Tirian G O, Filip I and Proştean G 2014 *Neurocomputing* **125** 236–45
[9] Spierings T, Kamperman A, Hengeveld H, Kromhout J and Dekker E 2017 *AISTech 2017 Proc.* 1655–64
[10] Badri A B and Cramb A W 2002 *Steelmaking Conference Proceedings* (Warrendale, PA: Iron and Steel Society) pp 65–76
[11] Thomas B G and Okelman M 2011 *Sensors, Sampling, Simul. Process Control* 127–34
[12] Zappulla M L S, Cho S M and Thomas B G 2019 *Steel Res. Int.* **90**
[13] Hibbeler L C, Chin See M M, Iwasaki J, Swartz K E, O'Malley R J and Thomas B G 2016 *Appl. Math. Model.* **40** 8530–51